2018 IEEE 15th International Symposium on Biomedical Imaging (ISBI 2018)
April 4-7, 2018, Washington, D.C., USA

DISSECTING BRANCHIOMOTOR NEURON CIRCUITS IN ZEBRAFISH — TOWARD HIGH-THROUGHPUT AUTOMATED ANALYSIS OF JAW MOVEMENTS

Yasmin M. Kassim[1*], *Noor M. Al-Shakarji*[1⋆], *Emilia Asante*[2⋆], *Anand Chandrasekhar*[2], *K. Palaniappan*[1]

[1]Computational Imaging and VisAnalysis (CIVA) Lab
Department of Electrical Engineering and Computer Science
[2]Division of Biological Sciences and Bond Life Sciences Center
University of Missouri-Columbia, Columbia, MO 65211 USA

ABSTRACT

We use the zebrafish model to understand brain circuits containing branchiomotor neurons that control jaw movements in vertebrates. In one approach, we compare circuit output, evaluated by dynamic analysis of jaw movement from video recordings, between wildtype zebrafish and mutants with specific circuit defects. While such analyses have been informative, they require extensive manual annotation. We developed an automated image analysis system to extract deformable motion features using video microscopy, for rapid and accurate detection of jaw movement termed *gape* or mouth opening. The approach uses a robust fusion process combining multiple local deformable motion models into a likelihood response trace curve followed by peak processing to reliably detect jaw movement. Performance on 24 labeled videos of zebrafish larvae across three age groups achieved 97.2% recall, 93.5% precision and 98.7% accuracy. The automated system demonstrates high fidelity *gape* analysis scalable for high-throughput studies in neuroscience and pharmacology.

Index Terms— Zebrafish, branchiomotor circuit, behavior, video microscopy, optical flow, background subtraction, motion map

1. INTRODUCTION & MOTOR NEUROCIRCUITRY

Chewing and swallowing are essential motor functions involving the coordination of jaw, other pharyngeal muscles and associated brain neural circuits that are controlled by branchiomotor (BM) neurons located in the brainstem [1, 2]. Defects in these motor functions (dysphagia) are often associated with neurological diseases like Parkinson's and amyotrophic lateral sclerosis (ALS) or Lou Gehrig's disease [3–5]. Although the organization and development of the branchiomotor neurons have been studied extensively [1, 2, 6], the formation and functional outputs of the neural networks driving jaw muscle movement have received less attention. Imaging-based studies to understand organism level behaviors using the zebrafish model system is receiving increased attention [7–11]. Advances in computational neuroscience and high-throughput imaging to investigate phenomics of model systems like zebrafish (*Danio rerio*), can provide insight into functional deficits such as chewing problems arising from aging and neurological disorders. In this study, we analyzed jaw movement and mouth opening or *gape* dynamics by video microscopy of zebrafish larvae followed by manual annotation and morphology analysis as shown in Figure 1. Jaw movement results in the opening of the mouth, termed the *gape*, which was manually outlined using contours in every movie frame. Gape area is a measure of the extent of mouth opening, that becomes very robust and periodic in older larvae.

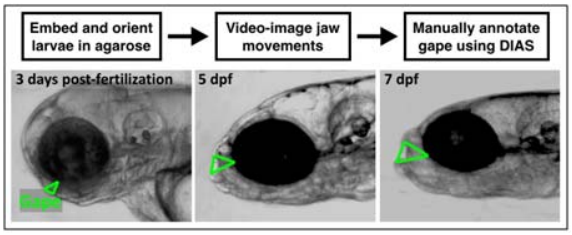

Fig. 1. Manual workflow for zebrafish jaw movement analysis using DIAS [12]. Gape feature (green) is outlined manually in individual frames of movies of 3 dpf, 5 dpf, and 7 dpf larvae.

We documented differences in gape frequency (rate of mouth opening) between wildtype larvae and a genetic mutant containing branchiomotor circuit defects. However, due to the bottleneck in manual annotations, these analyses were performed at low frame rates and for short durations. To address this issue, we created an image processing pipeline to facilitate automated high-throughput jaw movement analysis of videos captured at high frame rates and long duration. We combine two motion analysis methods: robust optical flow and background subtraction, using a unique robust fusion process that accurately detects gape or mouth opening events. Automated image analysis estimated gape frequencies that were very similar to those obtained manually.

*These authors contributed equally.

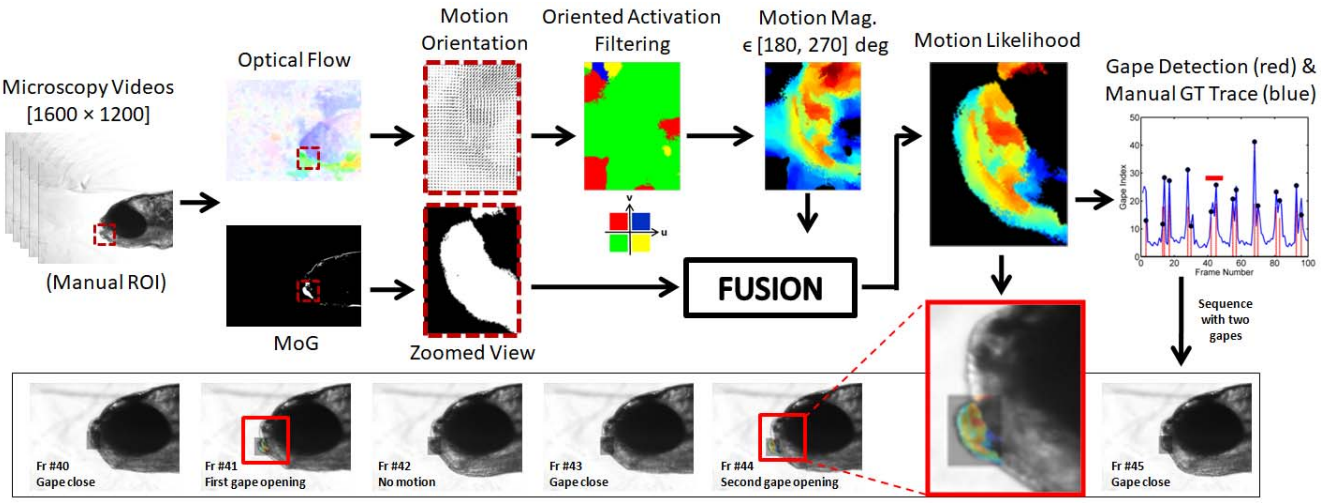

Fig. 3. System diagram for high-throughput image analytics pipeline for zebrafish larval jaw movement and gape frequency analysis using motion estimation and fusion. Region of interest (ROI) for gape is manually specified in the first frame.

Zebrafish Branchimotor (BM) Neurons: Figure 2 shows the organization and connectivity of the branchiomotor circuit visualized using transgenic zebrafish expressing green and red fluorescent proteins in jaw muscles and branchiomotor neurons, respectively. By 3 days post-fertilization (3 dpf), the axons of the branchiomotor neurons (red) have arrived at their targets, the jaw and gill muscles (green), and synapse formation is underway [13]. We genetically perturbed the organization of the BM neurons by interfering with neuronal migration during development and these mutant zebrafish larvae exhibited variations in gape frequency. Such phenotype perturbation studies enable the understanding and reverse engineering of how neuronal circuits control movement.

Our contributions include: (a) Analyzing zebrafish microscopy videos using multiple motion estimation models of articulated jaw movements; (b) Robustly fusing these noisy motion estimates to produce a likelihood map that characterizes gape opening events; and (c) Quantitatively assessing our automated gape measurement with annotations from expert biologists. Rest of the paper is organized as follows. Section 2 describes zebrafish articulated motion estimation methods and the detailed steps in our robust fusion process for analyzing motion fields. Section 3 describes the evaluation metrics, Section 4 summarizes the experimental results including comparison to manual ground truth, followed by Conclusions.

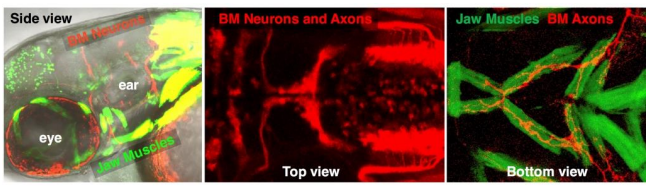

Fig. 2. Side, top and bottom views of branchiomotor neurons and axons (red) and jaw and gill muscles (green) in 3 dpf zebrafish larvae.

2. DEFORMABLE JAW MOTION ANALYSIS

Our automated image processing pipeline using deformable motion estimation is shown in Figure 3 (using 9-dpf, video5, WT as a sample sequence). The input to the pipeline are microscopy video frames and the output is a gape index trace plot that is used to determine zebrafish jaw frequency using a peak identification process. Multiple motion estimation combined with robust fusion is used to reliably merge motion fields and separate global from local motions. Our automated output has multiple responses in successive frames owing to the fact that the zebrafish larvae can take multiple (3 to 5) frames to open its mouth. We have implemented a peak identification process as a post-processing step to detect the maximum response over successive frames while considering the possibility of fast opening, closing and reopening behaviors which usually occurs more frequently in wild type zebrafish.

2.1. Multiple Motion Models of Jaw Movements

In order to accurately track the zebrafish larvae jaw movement behavior we apply a multiple motion estimation based approach followed by fusion. Optical flow estimation is a widely used method for motion detection and filtering. In this paper, we used the approach proposed in [14] and [15] for robust motion flow estimation. It uses a variational formulation incorporating vector median filtering to denoise the flow while preserving the energy in the final resultant field using weighted neighborhood image regions. We set the boundary pixels and associated derivative values moving outside of boundaries to zero. Motion feature maps are useful for segmenting the mouth region of interest (using manual ROI initialization). The objective function below estimates the horizontal, $\mathbf{u}$, and vertical, $\mathbf{v}$, components of the optical flow field from a pair of images $I(t)$ and $I(t+1)$, [14], where λ is a regularization parameter, ρ_D and ρ_S are robust statistics

penalty functions for the data and spatial terms respectively, and $\hat{\mathbf{u}}$ and $\hat{\mathbf{v}}$ are the auxiliary flow fields used in the last two terms to promote discontinuity preserving smoothing by approximate median filtering:

$$\begin{aligned} E(\mathbf{u},\mathbf{v},\hat{\mathbf{u}},\hat{\mathbf{v}},t) = & \\ & \sum_{i,j}\{\rho_D(I(i,j,t)-I(i+u_{i,j},j+v_{i,j},t+1)) \\ & +\lambda[\rho_S(u_{i,j}-u_{i+1,j})+\rho_S(u_{i,j}-u_{i,j+1}) \\ & +\rho_S(v_{i,j}-v_{i+1,j})+\rho_S(v_{i,j}-v_{i,j+1})]\} \\ & +\lambda_2(||\mathbf{u}-\hat{\mathbf{u}}||^2+(||\mathbf{v}-\hat{\mathbf{v}}||^2) \\ & +\sum_{i,j}\sum_{(i',j')\in N_{i,j}}\lambda_3(|\hat{u}_{i,j}-\hat{u}_{i',j'}|+|\hat{v}_{i,j}-\hat{v}_{i',j'}|)\ . \end{aligned} \tag{1}$$

In addition to optical flow field estimates, we incorporated a background subtraction model to filter out responses generated by global animal movement within the cropped region. The role of global motion filtering is to isolate responses only in places where the jaw is undergoing articulated motion. For a unimodal Gaussian background density estimate for the current frame, we estimate the pixel level time dependent background mean, $\mu(i,j,t)$, and variance, $\sigma^2(i,j,t)$, as:

$$\mu(i,j,t+1) \quad = \alpha I(i,j,t)+(1-\alpha)\mu(i,j,t) \tag{2}$$

$$\begin{aligned} \sigma^2(i,j,t+1) = \alpha(I(i,j,t)-\mu(i,j,t))^2+ \\ (1-\alpha)\sigma^2(i,j,t)\ . \end{aligned} \tag{3}$$

Parameter sweeping identified a foreground threshold of 0.3 using the first ten frames as the initial background model. This can be extended to a Mixture of Gaussian (MoG) model for more complex multimodal backgrounds.

2.2. Proposed Robust Fusion of Motion Fields

Multiple motion fields are fused assuming independent statistics of detection. The timevarying optical flow fields, $\mathbf{u}(t)$ and $\mathbf{v}(t)$ are combined with background subtraction responses, $\boldsymbol{\mu}(t)$ in those regions where the flow vectors, $\boldsymbol{\theta}(t)$, are appropriately oriented in the southwest direction, then we compute the fused gape likelihood response 1-D signal, $G(t)$,

$$\begin{aligned} G(t) = & \sum_{(i,j)\in N_{i,j}}(u_{i,j}^2(t)+v_{i,j}^2(t))^{0.5} \\ & \cdot|I(i,j,t)-\mu(i,j,t)|/\sigma(i,j,t))\cdot\delta_{SW}(\theta_{i,j}(t)) \end{aligned} \tag{4}$$

as the integrated value within the (cropped) jaw region using our unique robust fusion equation. The jaw region of interest can be identified using template methods or manually specified in the first frame. The cropped region usually has flow vectors in different directions due to fish muscle movement. These movements may result in large motion detections for the jaw region and lead to false positive gape responses. To mitigate this problem, we apply the robust motion fusion function based on Eq. 4 with the following characteristics:

1. Analyze the 2-D optical flow vectors (u,v) in the mouth ROI to extract four directional motion maps.
2. Oriented activation. Keep only one filtered region consistent with the desired direction of jaw movement.
3. Compute the magnitude of the flow field in jaw ROI.
4. Mask the magnitude (Step 3) with the filtered region (Step 2) to get the motion magnitude map in the ROI.
5. Fuse the masked magnitude (Step 4) with background subtraction in the ROI to filter out noisy responses.
6. Compute ROI fused motion likelihood map, to estimate a single variable response plot of gape index vs time.

3. QUANTITATIVE PERFORMANCE EVALUATION

The performance of the automated gape detection image processing pipeline was evaluated by comparison with manually labeled video frames referred to as ground-truth (GT). Three statistical measures were scored including recall (sensitivity), precision and accuracy defined as follows:

$$Recall = \frac{TP}{TP+FN} \tag{5}$$

$$Precision = \frac{TP}{TP+FP} \tag{6}$$

$$Accuracy = \frac{TP+TN}{TP+FP+FN+TN}\ . \tag{7}$$

An additional quantity to assess accuracy of the automated system is to measure the absolute difference in gape counts,

$$Gape_{count} = |GT_{gapecount} - \text{Automated}_{gapecount}|\ . \tag{8}$$

4. EXPERIMENTAL RESULTS AND DISCUSSION

We started out by testing whether jaw movements were affected in a zebrafish (*Danio rerio*) mutant where a subset of the BM neurons are mispositioned due to a failure in neuronal migration [16] (see Figure 4). While jaw movement was robust in mutants, gape frequency was much lower in a 7 dpf mutant larva (blue trace, 4+/-1 gapes/20 sec, N=19 larvae) compared to a wildtype larva (red trace, 14+/-3 gapes/20 sec, N=20 larvae); see Figure 4 (bottom). This mutant line with mispositioned BM neurons exhibited reduced gape frequency. Our aim is to use high-throughput imaging methods to characterize gape frequency phenotypes of mutations and pharmacological treatments that affect the connectivity or function of the branchiomotor circuits, potentially leading to variations in jaw movement.

Zebrafish were maintained in state-of-the-art aquarium facilities and all experiments were carried out under protocol #8825 approved by the Animal Care and Use Committee at the University of Missouri. The following transgenic lines were used: Tg(isl1:gfp) [13]; Tg(act1:gfp) [17]; Tg(zcrest:mrfp) [18]. The *off limits* (olt^{rw689}) neuronal migration mutant [16] was maintained in the Tg(isl1:gfp) background. The imaging protocol for dynamic analysis of jaw

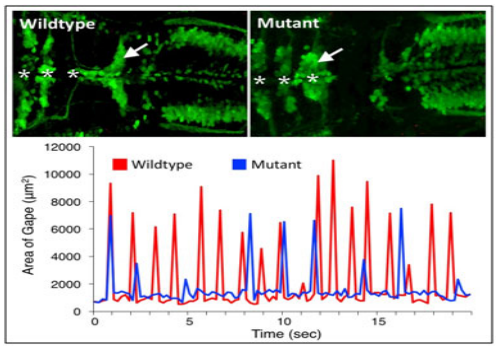

Fig. 4. Top row shows wildtype (normal) and mutant larval brains with mispositioned BM neurons (white arrows). The gape frequency (number of peaks per 20 sec) is reduced in the mutant larva (blue) compared to the wildtype (red).

movements in zebrafish used larvae between the ages of 3 to 9 days post-fertilization (dpf), embedded in 2% low-melting point agarose (Sigma) dissolved in E3 embryo medium [19], with the jaw region able to move freely (see Figure 1). Jaw movements were imaged under brightfield with an Olympus SZX12 stereo microscope (90X magnification) fitted with a Retiga 2000 camera (QImaging, Inc.), and videos were recorded at 1600×1200×8.33 frames per second at 12-bits per pixel for 12 seconds. The 100-frame movies were manually analyzed by tracing using Dynamic Image Analysis System (DIAS) software [12]. Jaw movement based on extent of mouth opening, termed the gape, was manually outlined in every movie frame and used as the labeled ground-truth.

Our analysis pipeline was tested on 24 zebrafish microscopy videos at three different larval time points including 7 videos from 5 dpf, 10 videos from 7 dpf (5 Wildtype and 5 Mutant) and 7 videos from 9 dpf. These videos were selected by biologists to evaluate the efficiency of our pipeline. The performance of the automatic method was evaluated using recall, precision, accuracy and absolute difference of counts compared to the gold standard manually labeled videos by biologists. Table 1 provides the average count and standard deviation for each age (5,7,9)-dpf category; the last row is the overall average and standard deviation across all videos.

Table 1. Quantitative gape evaluation at the frame correspondence level for three different age groups of zebrafish larvae.

Strain	#vid	Recall %	Precision %	Accuracy %
Avg 5-dpf	7	97.6 ± 6.3	92.4 ± 8.1	98.7 ± 1.4
Avg 7-dpf	10	96.1 ± 4.7	95.4 ± 4.5	98.7 ± 1.2
Avg 9-dpf	7	98.4 ± 4.2	91.8 ± 8.5	98.7 ± 1.4
Average	24	97.2 ± 4.9	93.5 ± 6.8	98.7 ± 1.2

The overall recall of 97.2% is higher than the overall precision of 93.5% indicating that our method rarely misses an event, but has more false positives. The latter is due to uncontrolled deformable fish motion and background agarose medium fluid motion; this could be handled using ROI tracking [20] or shape segmentation [21]. Gape counts range between 4 and 25 while the maximum error in gape count is 3 openings (Figure 5, negative gray bars). Figure 6 shows temporal visualizations of our automated gape extraction results (red) compared to manual tracing results (blue), with black dots marking jaw opening gape events. The automatic detections are accurate in number of gape events and well synchronized temporally with the GT trace and gape localization.

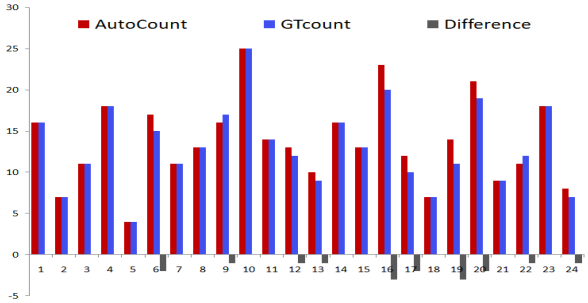

Fig. 5. Plot of gape count *vs* video number showing that automated extraction of gape is reliable across 24 different sequences; gray color (negative) bars are the differences in gape count between automated and manual results (Eq. 8).

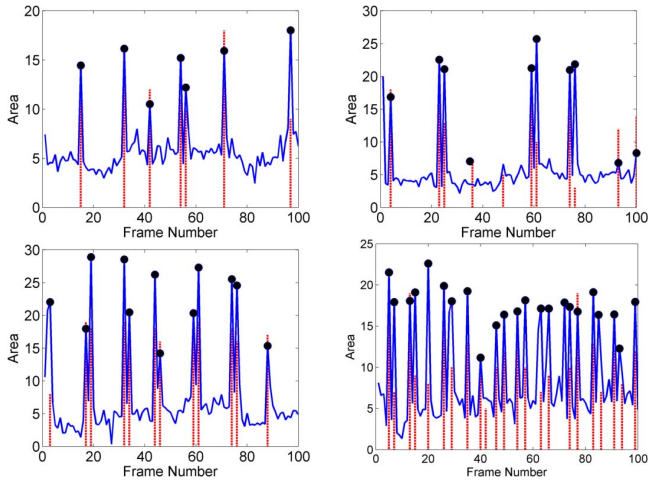

Fig. 6. Plot of gape area *vs* time for two mutant and two wildtype gape plots with automated results (red) superimposed on biologist manual tracing using DIAS (blue) and ground-truth (GT) gape events marked as black dots: (a) UL: 7-dpf Mutant4 (1.0, 1.0, 1.0), (b) UR: 7-dpf Mutant6 (0.91, 0.91, 0.98), (c) LL: 7-dpf Wildtype5 (1.0, 1.0, 1.0), and (d) LR: 7-dpf Wildtype10 (0.96, 0.96, 0.98) with (Recall, Precision, Acc).

5. CONCLUSIONS

The long-term objectives of our research is to examine how aging, disease and injury affect the functional organization and output of the branchiomotor circuits. In this paper, we have developed an automated video microscopy tool for measuring jaw movement behavior, specifically gape or mouth opening, at the organism level across different developmental time points. Our proposed method utilizes two motion analysis algorithms, optical flow and background subtraction, and

combines the motion estimates using a robust fusion process with peak detection using non-maximum suppression. The proposed fusion helps us to eliminate motion vectors in uninformative directions and to retain only a specific orientation correlated with the gape event within the selected ROI. Using our tool, we extracted gape frequency from 24 video sequences comprising 2400 frames of different individuals. The results are promising based on precision-recall performance measures, and compare favorably with manual annotation. The currently implemented tool will enable high-throughput dynamic analysis of the branchiomotor neural circuit output (i.e., jaw movement) in response to a broad spectrum of physical, chemical and genetic factors. For future work, the tool will be enhanced to automatically locate the jaw ROI in video recordings, extract deformable motion parameters and identify morphological features, not amenable to manual annotation. This will facilitate discovery of novel jaw dynamics of biological relevance with potential translational applications to pharmacology, neurophysiology and neuropsychiatry.

6. ACKNOWLEDGMENTS

Research supported by funds from the Bond Life Sciences Center and the University of Missouri (URC-17-078-n) to AC and partially by NIH R33EB00573 (KP).

7. REFERENCES

[1] Anand Chandrasekhar, "Turning heads: Development of vertebrate branchiomotor neurons," *Developmental Dynamics*, vol. 229, no. 1, pp. 143–161, 2004.

[2] Sarah Guthrie, "Patterning and axon guidance of cranial motor neurons.," *Nature Reviews Neuroscience*, vol. 8, no. 11, 2007.

[3] M.P. Jani and G.B. Gore, "Swallowing characteristics in amyotrophic lateral sclerosis," *NeuroRehabilitation*, vol. 39, no. 2, pp. 273–276, 2016.

[4] J.R. Kane and *et al.*, "Assessing the role of dopamine in limb and cranial-oromotor control in a rat model of parkinson's disease," *Journal of Communication Disorders*, vol. 44, no. 5, pp. 529–537, 2011.

[5] H.W. van Bruggen and *et al.*, "Predictive factors for masticatory performance in duchenne muscular dystrophy," *Neuromuscular Disorders*, vol. 24, no. 8, pp. 684–692, 2014.

[6] Andrew Lumsden and Robb Krumlauf, "Patterning the vertebrate neuraxis," *Science*, vol. 274, no. 5290, pp. 1109–1115, 1996.

[7] C. Cario and *et al.*, "Automated measurement of zebrafish larval movement," *The Journal of Physiology*, vol. 589, no. 15, pp. 3703–3708, 2011.

[8] R. Peravali and *et al.*, "Automated feature detection and imaging for high-resolution screening of zebrafish embryos," *Biotechniques*, vol. 50, no. 5, pp. 319, 2011.

[9] W. Spomer and *et al.*, "High-throughput screening of zebrafish embryos using automated heart detection and imaging," *Journal of Laboratory Automation*, vol. 17, no. 6, pp. 435–442, 2012.

[10] O. Rinner and *et al.*, "Contrast sensitivity, spatial and temporal tuning of the larval zebrafish optokinetic response," *Investigative Ophthalmology & Visual Science*, vol. 46, no. 1, pp. 137–142, 2005.

[11] O. Stern and *et al.*, "Automatic localization of interest points in zebrafish images with tree-based methods," *Pattern Recognition in Bioinformatics*, pp. 179–190, 2011.

[12] D.R. Soll and *et al.*, "Computer-assisted systems for the analysis of amoeboid cell motility," *Cytoskeleton Methods and Protocols*, pp. 45–58, 2001.

[13] S. Higashijima and *et al.*, "Visualization of cranial motor neurons in live transgenic zebrafish expressing green fluorescent protein under the control of the islet-1 promoter/enhancer," *Journal of Neuroscience*, vol. 20, no. 1, pp. 206–218, 2000.

[14] Deqing Sun, Stefan Roth, and Michael J Black, "Secrets of optical flow estimation and their principles," in *IEEE Conference on Computer Vision and Pattern Recognition*, 2010, pp. 2432–2439.

[15] K. Palaniappan, H. S. Jiang, and T. I. Baskin, "Nonrigid motion estimation using the robust tensor method," in *IEEE CVPR Workshop on Articulated and Nonrigid Motion*, 2004, vol. 1, pp. 25–33.

[16] H. Wada and *et al.*, "Frizzled3a and celsr2 function in the neuroepithelium to regulate migration of facial motor neurons in the developing zebrafish hindbrain," *Development*, vol. 133, no. 23, pp. 4749–4759, 2006.

[17] S. Higashijima and *et al.*, "High ferequency generation of transgenic zebrafish which reliably express GFP in whole muscles or the whole body by using promoters of zebrafish origin," *Developmental Biology*, vol. 192, pp. 289–299, 1997.

[18] O.M. Mapp and *et al.*, "Prickle1b mediates interpretation of migratory cues during zebrafish facial branchiomotor neuron migration," *Developmental Dynamics*, vol. 239, no. 1596–1608, 2010.

[19] Monte Westerfield, *The Zebrafish Book*, Eugene, OR: University of Oregon Press, 1995.

[20] N.M. Al-Shakarji and *et al.*, "CS-LoFT: Color and scale adaptive tracking using max-pooling with Bhattacharyya distance," in *IEEE Applied Imagery and Pattern Recognition Workshop*, 2016.

[21] Y.K. Kassim and *et al.*, "Random forests for dura mater microvasculature segmentation using epifluorescence images," in *IEEE Int. Conf. EMBS*, 2016, pp. 2901–2904.